ISSN 1063-7745, Crystallography Reports, 2022, Vol. 67, No. 2, pp. 236–251. © Pleiades Publishing, Inc., 2022.
Russian Text © The Author(s), 2022, published in Kristallografiya, 2022, Vol. 67, No. 2, pp. 278–294.

LATTICE DYNAMICS AND PHASE TRANSITIONS

The Second Stage of the α → γ Transformation during Slow Heating of Metastable Fe–Ni Alloys. Fine Structure of Dispersed γ-Martensite Plates

N. D. Zemtsova[a,*]

[a] *Institute of Metal Physics, Ural Branch, Russian Academy of Sciences, Yekaterinburg, 620041 Russia*

**e-mail: zemtsova@imp.uran.ru*

Received November 5, 2020; revised March 23, 2021; accepted September 24, 2021

Abstract—The structure of the Fe–Ni alloy formed in the initial stage of transformation of the internal structure of α crystal during heating has been analyzed. A complex multistep character of the formation of intermediate multilayer martensite phase ($3R + 18R + \varepsilon$) is established. Its formation mechanism is compared with the known behavior of the calorimetric slow heating curve of metastable Fe–32%Ni alloy, existing initially in the α + γ state.

DOI: 10.1134/S1063774522020249

INTRODUCTION

The phase transformations occurring during steel heating are based on the phenomenon of lattice polymorphism. The main regularities of polymorphic transformation determine the mechanism of phase transformations occurring during heating, including the formation of a new phase nucleus, its growth, and further dynamic transformation with an increase in temperature.

The Fe–Ni system is the key subsystem of many commercial nonmagnetic steels and alloys. The regularities of austenite formation during heating of metastable (Fe–Ni)-based alloys form an important section in the theory of steel thermal treatment [1, 2]. The necessary level of mechanical properties is obtained only under conditions of very slow heating of steel in the initial two-phase state α + γ with a rate of 0.2–0.4 K/min [2, 3]. In this paper, we report the results of studying the evolution of the structural state of α-martensite crystals during slow heating.

The mechanism of martensite–austenite transformation for Fe–Ni crystals is rather complicated; it includes several stages [4–6]. It was assumed in [3, 5, 6] as experimentally proven that the entire process of reverse martensite–austenite (α → γ) transformation upon slow heating of Fe–Ni alloys occurs in two stages. In the beginning of the temperature range of reverse transformation the mechanism of formation of dispersed austenite nanocrystals in α-martensite plates is similar to that of direct martensitic transformation: the same (Kurdjumov–Sachs, Nishiyama, or intermediate) orientation relationships are satisfied. Correspondingly, these nanocrystals were attributed to the γ-martensite phase. There are data that a dispersed intermediate ε phase can be formed in the beginning of the temperature range of α → γ transformation [3, 7], or even an advanced α → γ transformation may occur [8].

In the next (final) stage, in correspondence with the mechanism of diffusion bulk transformation, the two-phase mixture "residual α phase + γ martensite" is transformed into globular austenite. This mechanism of formation of fine-grained austenite structure suggests a smooth change in the physical characteristics of alloy during the α → γ transformation. However, the analysis of experimental data performed in [9] demonstrated inconsistency and nonlinearity of changes in the physical properties in the temperature range of the α → γ transformation in (Fe–Ni)-based alloys. The calorimetric curve (Fig. 1) [10] demonstrates especially clearly a sharply nonlinear α → γ transformation and gives grounds to divide this transformation at least into four stages, characterized by different development mechanisms.

The anomalous change in the physical characteristics was explained in [11]: it was assigned to the formation of large extended plates of a new phase (III stage) at the midpoint of the temperature range of reverse α → γ transformation. It was established in [11, 12] that these plates do not belong to the γ phase but form an intermediate phase ($3R + 9R$) of shear origin, which is induced by the energy of internal elastic stress in the two-phase (α + γ) martensite matrix (the $9R$ phase is the long-period phase of martensite type; the $3R$ phase is the γ phase, which accompanies the formation of the $9R$ phase according to the martensitic

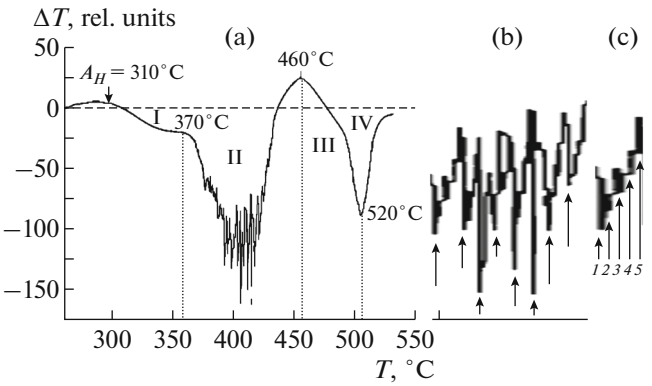

Fig. 1. Calorimetric effects revealed during slow heating of Fe–32.5%Ni alloy with a rate of 0.3 K/min [10]. (a) Complete curve (the temperature difference between the sample and reference is plotted on the ordinate axis, 25 rel. units = 0.125°C). (b) The range of 400–430°C, which corresponds to the most active formation of intermediate-phase crystals (arrows indicate the nucleation temperatures for new crystals). (c) The range of 400–404°C; arrows indicate the onset temperature of the (*1*) formation of γ-martensite plates, (*2*, *3*) relaxation processes in γ-martensite plates that lead to the formation of (*2*) ε martensite and (*3*) *R* martensite, and (*4*, *5*) twinning of intermediate-phase crystals over (*4*) a plane parallel to the habit plane and (*5*) a plane making an angle of 120° with it.

mechanism). Therefore, the phase composition of dispersed γ-martensite plates is doubtful, because their formation is preceded on the temperature scale by the occurrence of large extended plates of intermediate phase composition: the intermediate ($9R + 3R$) phase cannot arise after the equilibrium γ phase.

Moreover, up to this time, the interpretation of the results of studying the reverse transformation α → γ during heating of metastable Fe–Ni alloys has been based on the Fe–Ni phase diagram [13]. Being published even in 1979, this phase diagram [14] has remained for a long time without proper attention. Its important distinctive feature is the presence of ordered phases $L1_2$·Fe_3Ni and $L1_0$·FeNi, along with the $FeNi_3$ phase, which is present in all (known in the literature) Fe–Ni phase diagrams. It is fairly difficult to obtain convincing experimental results proving the presence of all these phases using structural methods; in particular, the efficiency of X-ray and electron diffraction techniques is low because of the proximity of the scattering factors of Fe and Ni atoms, which are neighbors in the Periodic Table.

Dispersed particles of precipitated phase in residual austenite phase and martensite crystals were detected by scanning electron microscopy (SEM) in [15, 16]. Their chemical composition, corresponding a particular phase (Fe_3Ni, FeNi, or Ni_3Fe) cannot be determined by electron backscatter diffraction, because the electron-probe diameter is an order of magnitude larger than the average size of precipitates; hence, along with the particles of interest, the probe captures a part of the surrounding matrix, consisting of the same chemical elements: Fe and Ni. The chemical composition of the precipitated phase was found from logical comparison of all existing data in [15, 16]. This phase turned out to be Fe_3Ni.

It was shown that even quenching of metastable Fe–Ni alloys (heated to high temperatures) from the austenitic region cannot prevent the segregation of the aforementioned phase. Specifically for this reason the opinion about the presence of an "immiscibility" region in the phase diagram dominates in the literature. This approach, implying stratification into components with low and high nickel concentrations in the structure of quenched alloys or the presence of regions with short-range atomic order, makes it possible to explain the invar properties of alloys.

During subsequent alloy cooling in liquid nitrogen (Fig. 2a) Fe_3Ni particles are transformed into α martensite, as can be seen in the SEM micrographs (Fig. 2b). In addition, it should be noted that α plates have a fragmented cellular structure (Fig. 2b); the cells are 0.3–1.0 μm in size. The cell boundaries are of disclination rather than dislocation origin. The martensite structure was analyzed in [17, 18]. It was shown that the fragmented structure of the peripheral part of initial martensite plates located on the sample surface is due to the superposition of the elastic stresses arising in the surrounding austenite and is shaped as a set of wedges starting from the interface and ending in the midrib region. This structure is formed as a result of the nucleation and motion of partial disclinations—structural defects, carriers of plastic deformation rotational modes—throughout the crystal.

Partial disclinations, interacting with the midrib twin structure, lead to the fragmentation of twins with subsequent shift and rotation of their fragments, thus violating the single twin zone (Fig. 2a). The structure presented in Fig. 2c is the result of this interaction; it indicates in no way the presence of ε phase at the points shown by arrows, as was suggested in [3, 7, 8]. In the sample bulk, under the conditions of uniform extension from the side of residual austenite, the fragmented misoriented structure of the peripheral part of α crystal becomes cellular (Fig. 2b). The contrast of the dark-field image of martensite structure in a transmission electron microscope is inhomogeneous, which is a manifestation of the martensite plate block structure.

According to the crystallographic analysis performed in [18], the block boundaries are traces of deformations occurring as a result of relaxation elastic stresses in the two-phase (α + γ) structure; the rotational modes of plastic deformation play a decisive role in the formation of these stresses. Due to this, the fragment boundaries do not belong to any crystallographic planes. This is evidenced by the mismatch of the misorientation angles of two conjugate fragments and boundaries of these fragments. Note that thin foils

prepared without heating in electrolyte (which often occurs but is disregarded) and, therefore, corresponding most closely to the structure of initial bulk samples, exhibit mainly disclination rotations of blocks in the martensite structure; i.e., their elastic conjugation.

In this study we made an attempt to eliminate (at least, partially) the contradictions in interpretation of experimental results and determine the structure of possible intermediate phases formed during the $\alpha \rightarrow \gamma$ transformation. Along with the own experimental results, data of many published studies, interpreted by the author, are also involved.

EXPERIMENTAL

The main experimental tool was transmission electron microscopy (TEM) of thin foils, because specifically this method makes it possible to determine martensite structures, as well as the types and values of inhomogeneous shifts in many cases where X-ray analysis cannot provide sufficiently accurate data.

After forging a Fe–32%Ni alloy was homogenized at 1100°C for 48 h and rapidly quenched in water. Cooling in liquid nitrogen and slow heating in air to room temperature led to the formation of ~80% α phase of athermal morphology. The reverse transformation $\alpha \rightarrow \gamma$ (A_H ~ 310°C [9]) was performed upon slow heating at a rate of 0.3 K/min from room temperature to different temperatures in the range of 370–520°C. Samples were cooled to room temperature in air. The initial sample size was 15 × 15 × 10 mm. Foil preforms were cut from the middle part of the samples by electric spark cutting, a technique introducing minimal distortions into the surface layer. The preforms were mechanically thinned to 0.2 mm using fine grinding paper, and then foils were fabricated in an electrolyte based on orthophosphoric acid (with chromic anhydride and sulfuric acid added) at a voltage of 25 V.

A structural analysis was performed at the Department of Electron Microscopy of the Testing Center of Nanotechnologies and Promising Materials (ITs NPM) (Institute of Metal Physics, Ural Branch, Russian Academy of Sciences) using a JEM-200CX TEM with a working voltage of 160 kV and a Quanta-200 SEM at room temperature. The joint use of two analytical methods made it possible to obtain more reliable and informative experimental data and establish a correspondence between the structural elements observed on local foil areas and in bulk samples.

RESULTS AND DISCUSSION

The first stage of the $\alpha \rightarrow \gamma$ transformation was investigated and described in detail in [15, 16]. Below we will consider briefly the mechanism of this stage.

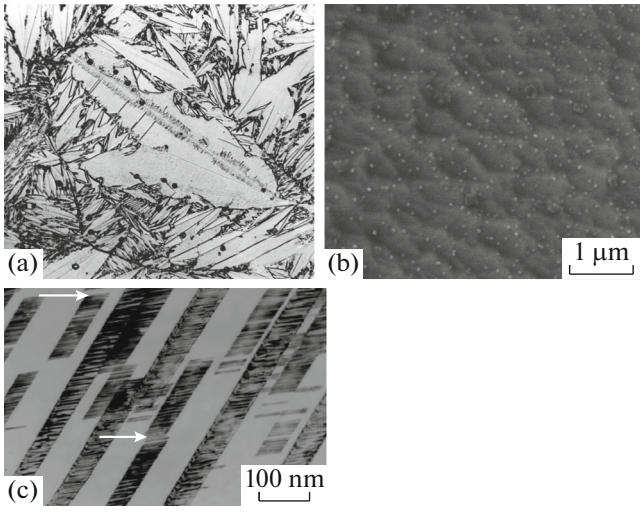

Fig. 2. Structure of Fe–32 at % Ni alloy in the initial $\alpha + \gamma$ state: (a) image obtained with an optical microscope, ×600 (one can see midrib-structure distortion in the region of its contact with the martensite crystal periphery); (b) the peripheral part recorded in SEM; and (c) the midrib region recorded in TEM [8].

Stage I

The growth of Fe_3Ni particles in residual austenite during slow heating with a rate of 0.3 K/min leads to an increase in the nickel content in the surrounding austenite and promotes the formation of a nucleus of discontinuous reaction {Fe_3Ni + γ-(Fe–Ni)} near the γ/α interface. The $\alpha \rightarrow \gamma$ transformation starts with migration of residual austenite boundaries towards martensite plates; it is accompanied by simultaneous occurrence of interrelated processes: coalescence of Fe_3Ni particles at γ/α interfaces and diffusion transport of nickel atoms from the bulk of martensite plates to interfaces. Coalescence of Fe_3Ni particles, which occurs intensively at γ/α interfaces, leads to a periodic distribution of coarsened particles, which makes possible migration of interface fragments free of Fe_3Ni particles. This leads to a change in the morphology of migrating interface: it turns from straight-line to bent, with teeth directed towards the α phase. As a result, the interface becomes jagged, which can also be easily observed in metallographic images. It was indicated in [19] that even no attempts had been made to explain the origin of interface jaggedness—one of unsolved questions concerning the structural mechanism of austenite formation upon heating. The nature of this phenomenon was reliably established only in [15, 16].

In alloys with a nickel content of 31–32% this discontinuous reaction of $\alpha \rightarrow \gamma$ transformation begins at 310°C [9, 10] but does not finish; i.e., the transformation is not completed. According to any published phase diagram, a necessary condition for its complete implementation is the supply of nickel atoms from the α-plate bulk to the migrating interface, which should

be provided by bulk diffusion. Since the bulk diffusion coefficient is small (3 orders of magnitude smaller than that along boundaries), a "buffer" layer is formed at the γ/α interface from the side of the α phase; this layer, depleted with nickel, is more stable with respect to the α → γ transformation, due to which the α → γ transformation according to this discontinuous mechanism stops. The first stage ends when reaches a temperature of ~370°C (Fig. 1). Finally, a high-nickel (up to 40% Ni) component arises in γ austenite; it is concentrated near γ/α interfaces, whose length significantly increases in view of the change in their morphology (jagged instead of straight-line).

Stage II

The formation of a nickel-depleted buffer layer in the α phase from the side of the α/γ interface brings the alloy to the second stage of α → γ transformation: dispersed new-phase crystals are formed in martensite crystals with orientations differing from that of the residual austenite.

The object of consideration in [2] was only the formation of dispersed γ martensite upon slow heating of steel in the α + γ state in the critical temperature range and the occurrence of globular austenite in the final stage of α → γ transformation. This analysis was supplemented in [3] by consideration of the formation of ε martensite under different conditions of heat treatment of the initial metastable Fe–Ni alloy in the α + γ state. The detection of ε phase in Fe–Ni alloys is puzzling, because this phase has never been observed previously in nickel and nickel–carbon austenitic steels with high energy of stacking faults. Let us consider some facts reported in [3, 7, 8]. The experimental data on the changes in the resistance and magnetization upon slow heating to 400°C [3, 8, 12] suggest that the volume fraction of the new paramagnetic phase cannot exceed 2.5%, whereas in the dark-field structure image presented in Fig. 5 in [8], which was obtained for the complex reflection $10\bar{1}_\varepsilon + 11\bar{1}_\gamma$, the exposed phase occupies maximally possible volume, covering almost completely the martensite plate. This inconsistency of the results indicates that the electron diffraction pattern was interpreted improperly. The electron diffraction pattern presented in Fig. 1 in [7] exhibits diffuse rods, whose origin was not discussed. Specifically their presence makes it possible to interpret correctly the electron diffraction pattern.

One must remember that martensite-type transformations occur as a result of cooperative shifts of atomic planes, a consequence of which is rigorous mutual orientation of the martensite phase relative to the initial one. Therefore, when interpreting an electron diffraction pattern, it is insufficient to determine only interplanar spacings; it is also important to take into account that the γ phase and new intermediate phase were formed as a result of the shear phase transformation of martensitic type.

The structure of martensite-origin phases most often contains defects: the formation of martensite phases is accompanied by the occurrence of randomly arranged stacking faults, which are necessary for phase accommodation during martensitic transformation. Due to the presence of these defects, the stacking fault arrangement deviates from periodic, which leads to broadening of diffraction spots [20]. An increase in the number of violations in the periodic distribution of stacking faults causes a significant expansion of diffraction spots; they merge to form a continuous diffuse intensity band. Thus, if an electron diffraction pattern exhibits equally spaced and identically directed diffuse regions, they all are due to the presence of randomly arranged stacking faults in the phase structure of a single crystallographic orientation; this circumstance must be taken into account when interpreting an electron diffraction pattern.

Based on the nature of formation of diffuse rods in electron diffraction pattern, we can conclude that the reflections of the newly formed phase of each orientation are located on the corresponding diffuse rod, which arose specifically because of the randomly located stacking faults in the structure of this phase. In [7] the 100_ε and $10\bar{1}_\varepsilon$ reflections were attributed to different zone axes: $[001]_\varepsilon$ and $[121]_\varepsilon$, respectively. However, these reflections are located on the same diffuse rod; therefore, according to the martensitic transformation crystallography [21], they should belong to the same zone axis. Therefore, the electron diffraction pattern was interpreted improperly in [7]. In addition, the orientation relationship between the ε and γ phases, which would indicate their shear origin, was not determined. Moreover, the γ phase was also formed according to the martensitic mechanism in this case. Therefore, the reflections $0\bar{2}0_\gamma$ and 200_γ of the same type, corresponding to the same orientation of martensite crystal, cannot lie on the same diffuse rod: the $[00\bar{1}]_\gamma$ zone axis is absent. This electron diffraction pattern and the corresponding structural image will be interpreted below. The interpretation of the $1\bar{1}0_\gamma$ reflection as a superstructural one is incorrect.

The formation of dispersed crystals of new paramagnetic phase during slow heating has been established and accepted by many researchers [4–6, 11, 12]. Gorbach et al. [4] found a dispersed phase in α-martensite plates by the method of replicas, in view of which its lattice was not determined exactly, and its orientation relationship with the α-martensite lattice could not be revealed. This phase is a priori assumed to be austenitic. It was established most reliably in that study that from two to six austenite orientations arise within one martensite plate. The most widespread case is the occurrence of new-phase plates of four orientations.

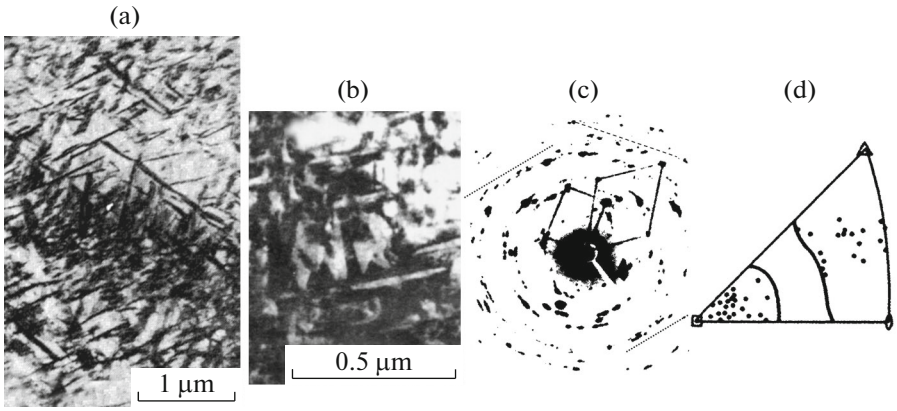

Fig. 3. Alloy structure images [2, 3]: (a) Fe–30 at % Ni after slow heating of the α + γ phase to 500°C; (b) N26KhT1 after partial transformation α → γ under isothermal conditions at 540°C; (c) the corresponding electron diffraction pattern (cells of $[110]_\alpha$ and $[41\bar{1}]_\gamma$ zone axes are selected); and (d) distribution (identical for both structures) of γ-phase orientations ($\{200\}_\gamma$ poles) after a cycle of γ → α → γ transformations in the coordinates of initial γ-phase.

However, a possibility of forming 24 orientations of dispersed γ martensite, nucleating within a single α-martensite crystal, was described much later in [2, 3, 22]. It was shown that, after a cycle of γ → α → γ transformations, the $\{200\}_\gamma$ poles of differently oriented dispersed thin lamellar austenite in the stereographic triangle of initial austenite are located in the calculation domains (outlined), allowed by the Kurdjumov–Sachs orientation relationships (Fig. 3). It was concluded that upon heating all γ orientations are observed in one α crystal, without any limitations; these orientations are allowed by the martensite orientation relationship.

Note that the electron diffraction pattern (Fig. 3c) [2, 3, 22], whose calculation yielded this very important information, was obtained for the structures of N30 and N26KhT1 alloys (Figs. 3a, 3b). Taking into account the magnification of the presented images and the electron beam diameter (~1 μm), one can conclude that the microdiffraction pattern was obtained for the entire structure, including not only the martensite plate: several plates of the second (and, maybe, even third) order are located between the two first-order plates. Therefore, the statement about the formation of new-phase plates with a set of orientations up to 24 in an α-phase plate is incorrect; however, the fact of shear formation of dispersed plates is proven (Fig. 3c), because their orientations obey the martensite orientation relationships, and the recorded reflections are located in the allowed regions of stereographic triangle (Fig. 3d).

The formation of dispersed new-phase crystals in α-martensite plates of Fe–32%Ni and Fe–25%Ni–1%Cr–2%Ti alloys upon slow heating with a rate of 0.3 K/min was revealed in [11, 12, 23]. The structure of martensite plates after slow heating, starting with 370°C, was investigated in this study by thin-foil TEM. The structure of α plates exhibited strict periodic striations (Fig. 4a), and the corresponding electron diffraction pattern (Fig. 4c) contained satellites, located equidistantly near each α-phase reflection. The zone axis was found to be $[110]_\alpha$. The satellite location line deviates from $[1\bar{1}0]$ by an angle of ~20°. A line parallel to the satellite location line is drawn near the zero spot. In the regions of α-phase structure with a changed orientation the orientation of modulated-structure planes changes as well: periodic striations are observed in other {110} planes: $(01\bar{1})$ and/or (101). This experimental fact is illustrated by arrows in Fig. 4a; for convenience, it is shown on enlarged scale in Fig. 4b.

As known from solid-state physics [24, 25], satellites are a manifestation of modulated structure in the arrangement of aging phase: periodic distribution of phases precipitating during solid solution decomposition into two phases with different concentrations and lattice parameters. The decomposition of this type is referred to as spinodal. Individual reflections from individual phases are not observed, because the entire solution scatters coherently. Satellites are formed near the main reflections, corresponding to a single-phase structure. The formation of this modulated structure with a period of ~100–200 Å is accompanied by the occurrence of elastic stress. The elastic stress energy in anisotropic solid solutions depends on the crystallographic direction. Therefore, the highest growth rate is observed in certain crystallographic directions, and the arising modulated structure is related to certain crystallographic axes.

The main difference of spinodal decomposition from the α → γ transformation is that the former implies precipitation of an isomorphic phase, with a parameter fairly close to that of the initial phase and differing only slightly from it, for example, by the

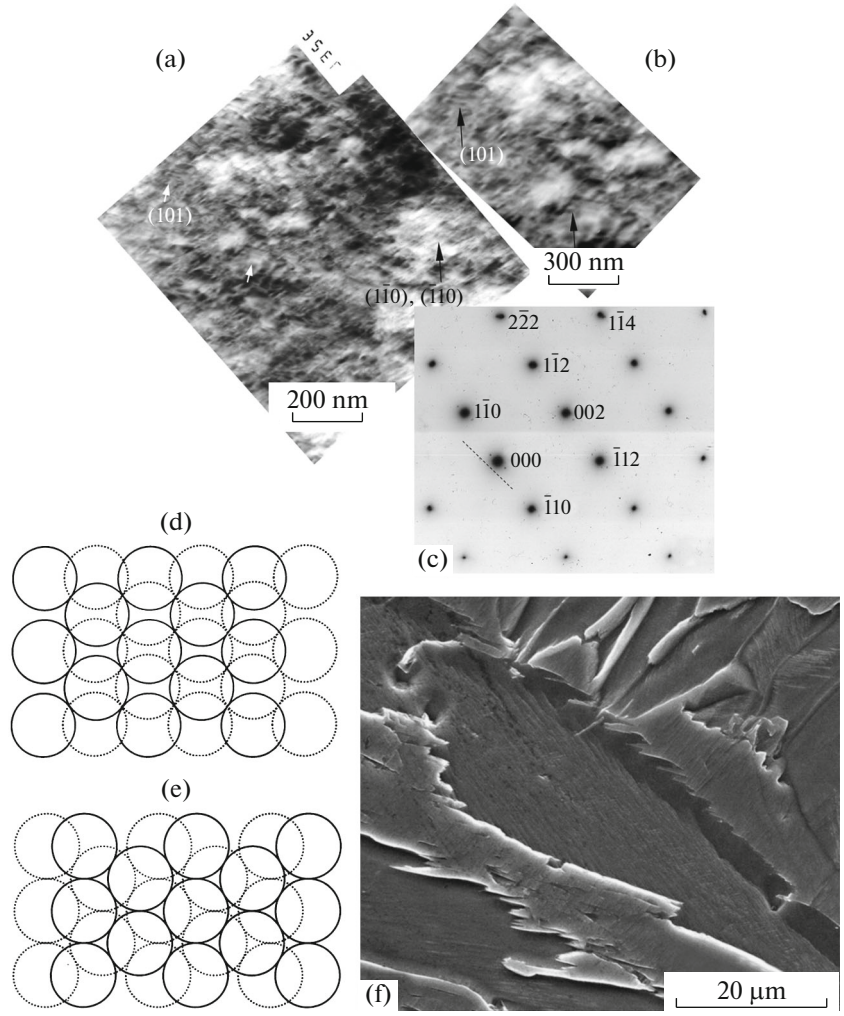

Fig. 4. Structure of an α plate after slow heating to 380°C: (a) modulated structure formed as a result of shear of (1$\bar{1}$0) or ($\bar{1}$10) planes; (b) enlarged structure fragment with another direction of plane shear; (c) the corresponding electron diffraction pattern (the satellite splitting direction deviates from [1$\bar{1}$0] by an angle of ~20°), (d, e) schematic of contraction displacement of (110)-type planes along the cube diagonal in the bcc lattice [28], average position in the initial state (d) and the corresponding structure of the plane of contact between fcc or hcp lattices and the bcc lattice of the initial phase (e); and (f) an SEM image of modulated structure in an α-martensite crystal.

occurrence of tetragonality. In the latter case a phase transformation with a change of lattice type occurs; however, the first stage of this process, as demonstrated in this study, is also the formation of a modulated structure via contraction displacement of {110} planes. The direction and magnitude of contraction displacements are determined by the tendency of atoms to move closer together and occupy energetically more favorable positions in the initial stage of the formation of new martensitic phase: thermal vibrations of {110} planes occur along the cube diagonal ⟨110⟩.

This process occurs spontaneously, without doing a work on the formation of new-phase nucleus, i.e., without overcoming the energy barrier. This is evidenced by the rather small deviation of the calorimetric curve from horizontal in the temperature range of 330–380°C (Fig. 1).

The same transformation regularities were obtained in [26] (where the theory of bcc → hcp and bcc → fcc transformations in metals and alloys with a bcc lattice was presented, with experimental confirmation by studying the diffuse X-ray scattering during sample cooling): a modulated structure, caused by the vibration of (110)-type planes along the diagonal cube direction [1$\bar{1}$0], is also formed in the first stage. Therefore, one can assume that the onset of the α → γ (bcc → fcc) transformation in binary metastable Fe–Ni alloys upon heating is consistent with the theory proposed in [26]. The schematic in Figs. 4d and 4e demonstrates the contraction displacement of (110) planes: the crystal tends to be packed as close as possi-

ble, eliminate interatomic gaps, and provide a maximum number of contacts between spheres. Figure 4d shows two neighboring planes of this type at the initial temperature; the viewpoint is such that one of them lies exactly in the drawing plane, while the other is behind it. Figure 4e presents the same planes in the case of formation of new-phase crystals. A comparison of these plots shows that the planes were slightly extended in the horizontal direction and slightly contracted in the vertical direction, became close-packed, and shifted with respect to each other. As a result of the bcc $\rightarrow$ *NR*, bcc $\rightarrow$ *NH*, or bcc $\rightarrow \gamma$ transformation, the (011) plane of loose (non-close-packed) bcc lattice passes to the hexagonal prism basal plane (0001), whose structure is equivalent to $(111)_{fcc}$ (*N* indicates the number of close-packed layers per unit cell in multilayer lattices of rhombohedral *R* or hexagonal *H* structures). Thus, the formation of new-phase crystals begins with shear contraction displacement of (110)-type planes along the $[1\bar{1}0]$ direction. There are six such sets in a bcc lattice; therefore, only 6 rather than 24 new-phase orientations may arise. Indeed, the number of experimentally observed versions of misoriented nanocrystals in a single α crystal has never exceeded six. Specifically this displacement of planes leads to a decrease in the specific volume of α phase, which is necessary for transformation of its loose (bcc) lattice into a denser lattice of new dispersed phase of martensitic nature. This pattern of the $\alpha \rightarrow \gamma$ transformation onset upon heating has been found for the first time.

The recorded deviation of (110) planes from the $[1\bar{1}0]$ direction by 20° is compatible with the requirement for symmetric arrangement of atoms in the basal plane {0001} of ε or *R* phases; it is caused, along with the tertragonality of martensite lattice, by the elastic strain field of the α-phase block structure. According to the data of [27], this angular deviation may reach ~35°.

If a martensite crystal has a favorable orientation, a modulated structure can also be seen in a SEM image of the sample surface (Fig. 4f). It is observed as a highly dispersed, striated structure, whose direction deviates from that of transformation twins in the midrib. Its unclear linearity is due to the presence of Fe_3Ni particles.

In Fig. 5 the region of disclination rotation of several martensite-plate blocks is in the most favorable reflection position. The α-phase zone axis is [111]. The electron diffraction pattern contains at least two systems of satellites, located only near the α-matrix reflections, practically in the same direction. The clearest reflection of the second satellite system is indicated by an arrow. Therefore, the modulated structure is formed only in the matrix undistorted by elastic stress. The intense reflections correspond to two orientations of intermediate-phase particles, formed in the disclination rotation region. The reflections from the latter correspond to neither γ nor ε phases. We will denote them as *R*.

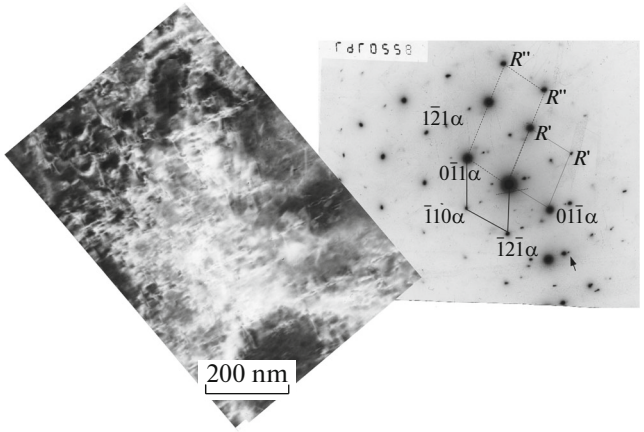

Fig. 5. Structure of disclination rotation region in a sample subjected to slow heating to 380°C: zone axis [111] of the α phase; its unit cell is outlined by solid lines; two systems of satellites can be seen near α-phase reflections, these systems are arranged almost in the same direction (dotted straight line near zero reflection, the reflection of the second satellite system is denoted by an arrow). The strongest reflections *R*' and *R*'' correspond to two orientations of intermediate-phase particles. Their cells are outlined by dashed and dotted lines.

All three aforementioned lattices have a common direction: $[1\bar{1}0]$, which indicates orientation relationship of the matrix with particles of both orientations, differing by the rotation angle with respect to the $[1\bar{1}0]$ direction. In the region of disclination rotation, which is characterized by a significant lattice curvature and elevated internal energy store, direct nucleation of intermediate-phase particles occurs, without preliminary formation of a modulated structure. This process corresponds to a range of ~370–400°C on the calorimetric curve (Fig. 1). With an increase in temperature, nucleation of new-phase particles in α-crystal blocks occurs as well.

Figures 6a and 6b show the structure of a martensite plate formed during slow heating to 400°C. The cellular martensite structure can be seen well due to the difference in the contrasts of individual blocks (Fig. 6b). However, unlike in Fig. 4, the blocks indicated by arrows (from above) exhibit two intersecting systems of striations, or two modulated structures formed by the $(0\bar{1}1)_\alpha$ planes (a trace of these planes lies in ~$[\bar{2}11]$, indicated by a dotted line) and $(\bar{1}01)_\alpha$ planes (a trace of these planes lies in ~$[1\bar{2}1]$, indicated by a dash-and-dot line). The modulated structure in the lower block is poorly distinguishable. In other blocks other {110} planes, undergoing thermal vibrations and subsequent stabilization, may be most preferred. The angle between the directions of striations—two systems of the modulated structure—is the angle

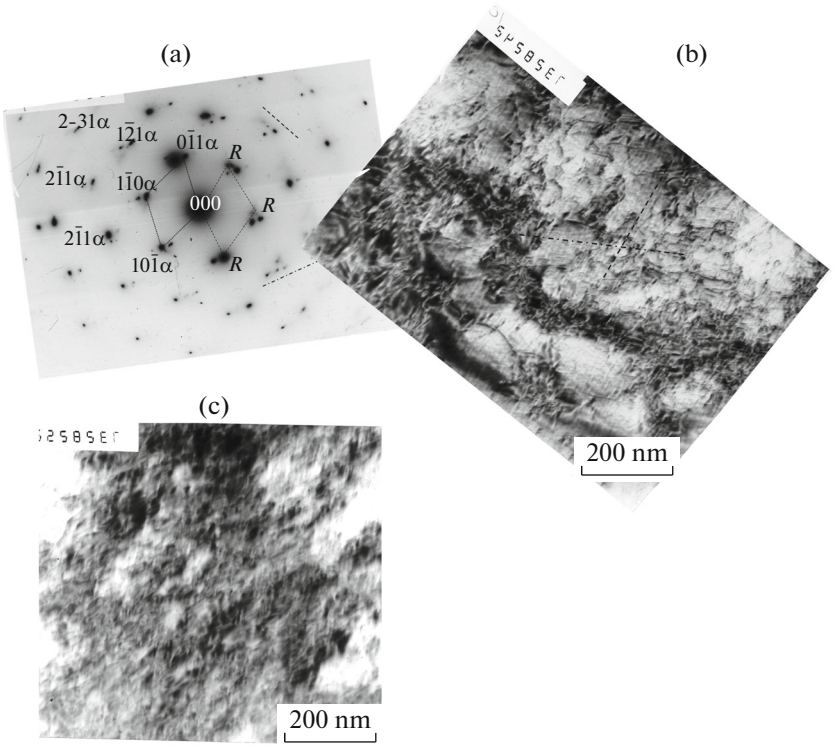

Fig. 6. Structure image of a martensite plate formed during slow heating to 400°C. (a) Electron diffraction pattern, zone axis $[111]_\alpha$, two satellite systems can be seen (the directions are indicated by dot-dashed and dotted lines); the *R*-phase reflections are connected with α-phase reflections by a strand. (b) Two modulated structures formed by $(\bar{1}01)_\alpha$ and $(0\bar{1}1)_\alpha$ planes, whose traces correspond to the satellite arrangement near α-phase reflections in the electron diffraction pattern (indicated by the corresponding lines); *R* phase in the form of dashes can be seen in the disclination rotation region. (c) Two modulated structures corresponding to another foil orientation.

between the lines containing satellites in the electron diffraction pattern; it differs only slightly (by ~5°) from the angle between the $[0\bar{1}1]_\alpha$ and $[10\bar{1}]_\alpha$ directions. This experimental fact proves the interdependence of the modulated striation systems in the structural image and the arrangement of satellites in the electron diffraction pattern.

Regular striations are not observed in the zone of block disclination rotation (Fig. 6b). One can see individual short multidirectional dashes, which are dispersed crystals of new intermediate phase: the intermediate phase nucleation on the path of reverse transformation α → γ is facilitated in the elastic field of block disclination rotation. In the electron diffraction pattern, this phase apparently corresponds to the reflections located near the α reflections and linked by a diffuse strand with them. This is indicative of shear mechanism of nucleation of the new phase; its reflections, which do not correspond to the γ phase, are denoted as *R* reflections. Since the modulated structure was observed in N32 alloy for the first time, we present its image (Fig. 6c), in which at least two systems of intersecting modulated structures can also be seen.

An increase in the final temperature of slow heating to 430°C (Fig. 7) leads to the formation of individual new-phase particles in the initial α-phase plates against the background of modulated structure. Lines parallel to the particle extension direction are drawn in the dark-field structural image from [7] obtained for the complex reflection indicated by an arrow in Fig. 7a (inset). The identity of lines reflects the small-angle misorientation of the particles formed in the martensite crystal. Different lines indicate the directions of diffuse rods in the electron diffraction pattern, which are due to the high density of random stacking defects, arising during the martensitic mechanism of new-phase formation. Note that each diffuse rod in the diffraction pattern is also split into several rods, which is especially pronounced in the enlarged reflection image in the lower inset in Fig. 7c. With this small-angle scattering neglected, we can indicate that the directions of diffuse rods in the electron diffraction pattern are orthogonal to the corresponding directions of dispersed phase extension.

The ε phase, suggested in [7], as well as the γ phase, is formed in an α matrix via the martensitic mechanism. The mechanism of *R*-phase formation is the

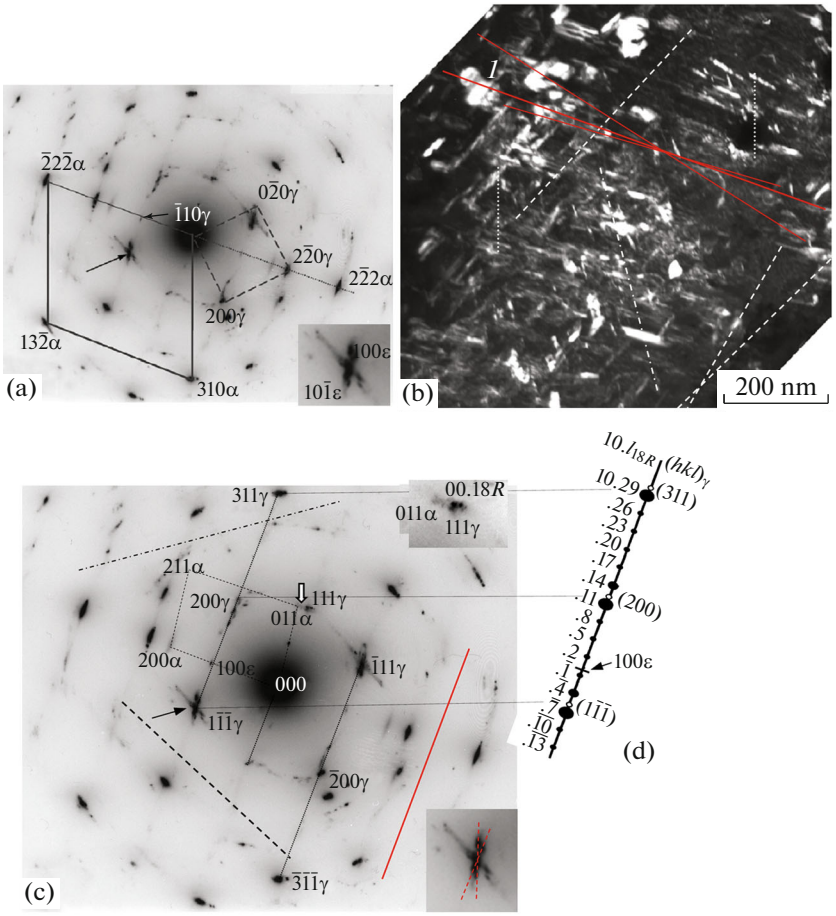

Fig. 7. (a, c) Electron diffraction patterns and (b) structure of Fe–32%Ni alloy after quenching for martensite and $\alpha \rightarrow \gamma$ transformation upon slow heating to 430°C at a rate of 0.2 K/min [7]: (a) networks of reflections from the $[1\bar{3}\bar{4}]_\alpha$ and $[00\bar{1}]_\gamma$ zone axes are selected; (b) dark-field image in a combined reflection (indicated by an arrow in panel (a)) and its interpretation in the bottom inset; (c) repeated panel (a) with interpretation; the top inset presents a group of reflections, indicated by a white arrow, a small-dash line indicates the α-phase zone axis $[01\bar{1}]_\alpha$ (the image contains lines oriented parallel to the particle extension direction, the diffuse-rod direction is presented in the electron diffraction pattern, the inset bottom shows their small-angle misorientation, corresponding to that of martensite crystals). (d) A site row of the reciprocal 18*R*-phase lattice; bright points indicate the location of fcc-phase sites, and dashes show the location of ε-phase reflection 100.

same. The γ, ε, and *R* phases are referred to as polytypes. The crystal structure of polytypes differs by only the alternation order of some atomic planes, whereas the structure of the planes (atomic arrangement) is identical for different polytypes of the same material. The mechanism of formation of ε and *R* phases in an fcc γ matrix at the atomic level is described in monograph [21]. The original methods for studying these structures (described previously in detail) and specific features of their diffraction pattern and calculation were used in this study; they served a basis for interpreting the results of electron microscopy analysis of the reverse transformation $\alpha \rightarrow \gamma$ in Fe–Ni alloys. We will briefly describe them below.

To clarify the lattice transformation geometry at the fcc $\rightarrow$ 9*R* and fcc $\rightarrow$ ε transitions, we will consider them in the hexagonal system of axes (Fig. 8). Figures 8a and 8b show three unit cells of the γ phase with a sequence of planes *ABC*... and one unit cell of the 9*R* structure with a sequence of planes *ABCBCACAB*.., which are oriented with respect to each other in correspondence with the experimentally found orientation relationships: $(111)_{fcc} \| (0001)_R$ and $[10\bar{1}]_{fcc} \| [11\bar{2}0]_R$ (close-packed planes and close-packed directions lying in these planes are parallel). A comparison of the atomic arrangement in these structures suggests that they differ in only the alternation order of close-packed planes *A*, *B*, and *C*. The 9*R* lattice consists of three "packets" of planes, which have an fcc sequence; all "packets" are shifted relative to each other by the Burgers vector of partial dislocation $a/6\langle 112\rangle$. One can see that a 9*R* structure can be obtained from an fcc lattice by shifting packets with a thickness of three (111) layers in the $\langle 112\rangle$ direction by a distance of $a/\sqrt{6}$.

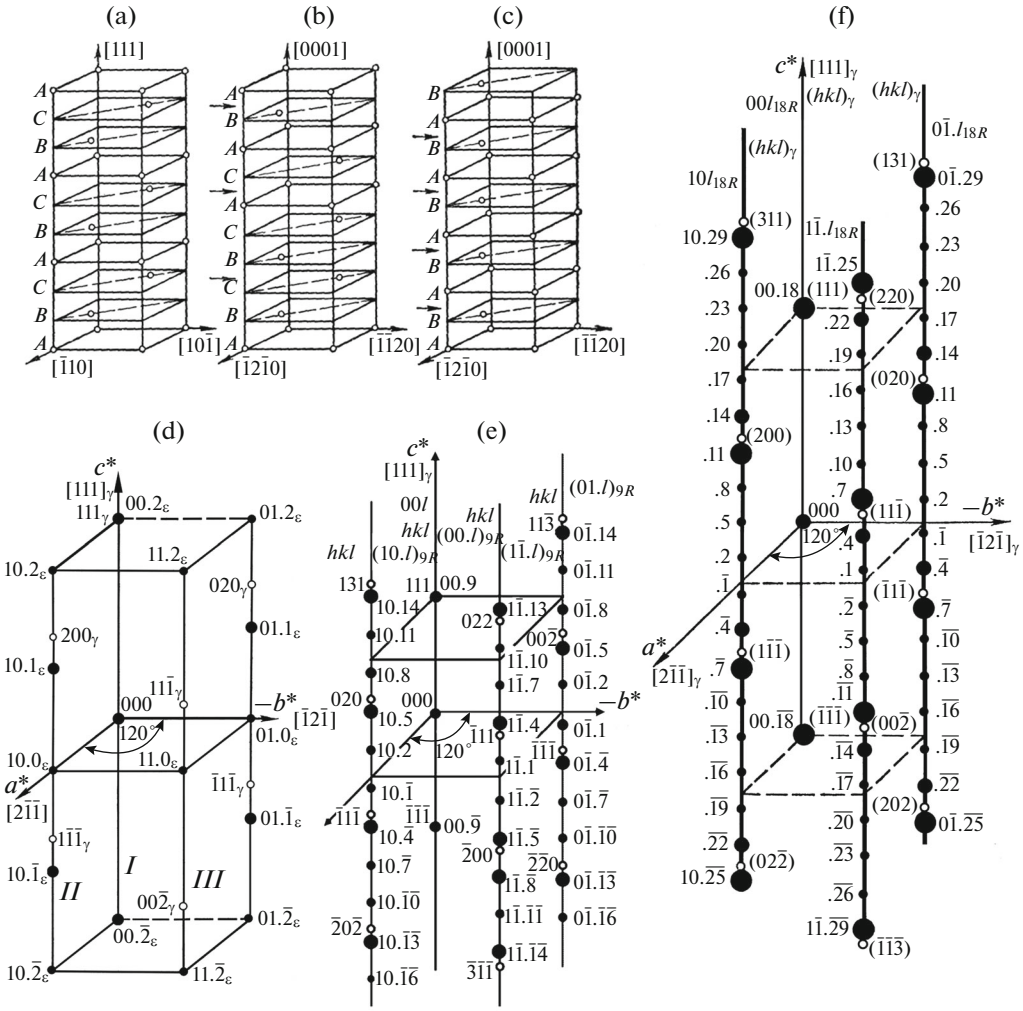

Fig. 8. Schematic of the formation from an fcc lattice (a) of close-packed 9*R* (b) and ε (c) structures in the hexagonal system of axes [21]. Joint reciprocal lattices of the fcc structure (bright circles): (d) ε martensite, (e) 9*R* martensite (solid line outlines 1/9 of unit cell), and (f) 18*R* martensite. The circle size is proportional to the structure factor.

These shifts give rise to deformation stacking faults. Therefore, the fcc → 9*R* transformation can be considered as the occurrence of periodic stacking faults after each third $(111)_{fcc}$ layer.

If periodic shifts occur after each second $(111)_{fcc}$ layer (Fig. 8c), the fcc → ε transformation is implemented, and a phase of hexagonal symmetry arises; the ε phase is denoted as 2*H*. Vice versa, if periodic shifts are implemented with a large period (e.g., after each six layers), the 18*R* phase is formed. In the general case the multilayer lattice of *R* phase is denoted as *NR*, where *N* is the number of cubic layers per *R*-phase unit cell. The reliability of the structural model of 18*R* phase as an fcc lattice with periodic shifts after each sixth $(111)_{fcc}$ layer was confirmed by calculation of diffraction pattern along the reciprocal lattice axis c^* [28, 29]: six additional maxima arise on a single period of fcc structure because of the periodic stacking faults.

Note that the hcp ε structure may contain periodic stacking faults, which transform hexagonal layers into cubic ones. Depending on their location frequency, 4*H*, 6*H*, 12*H*, and other phases are formed, which are denoted as *NH* (*N* is the number of hexagonal layers per *H*-phase unit cell).

For convenience of interpreting electron diffraction patterns of γ, ε (2*H*), or *R* phase, reciprocal lattices in the hexagonal system of axes are also used. To interpret the experimental results of this study, focused on the analysis of the α → γ transformation in metastable Fe–Ni alloys, in which the occurrence of a dispersed phase is always accompanied by the formation of γ phase, we present joint reciprocal γ-phase lattices with each of suggested phases (ε, 9*R*, and 18*R*) in the hexagonal system of axes (Figs. 8d–8f). Helpful is the use of a comparative scheme of arrangement of lattice sites along 10ℓ rows, lying in the (010) plane of multilayer *NH* and *NR* lattices relative to the 3*R* sites of γ

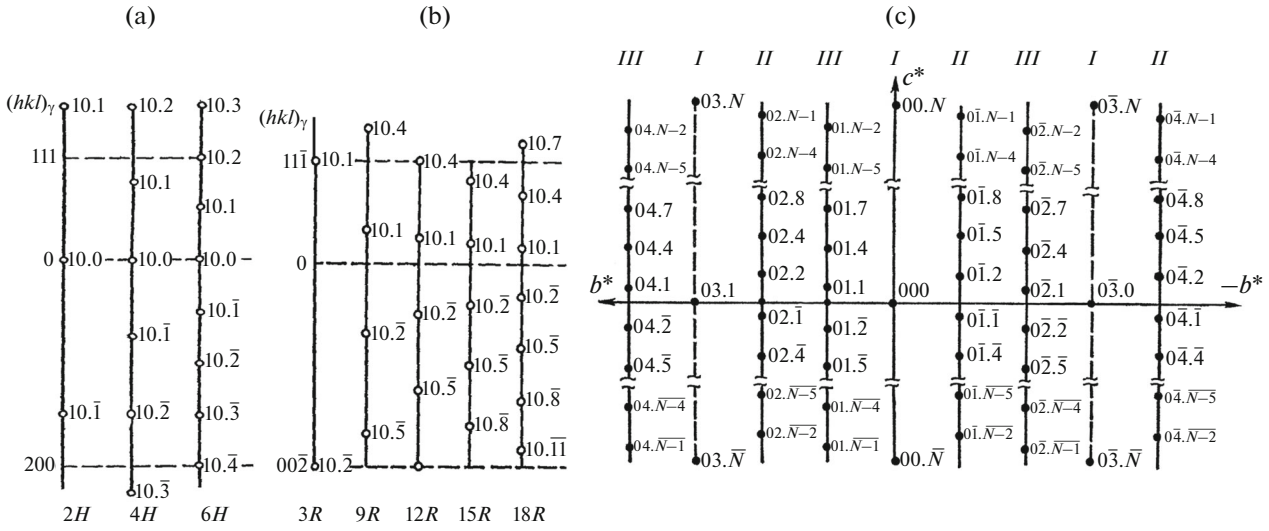

Fig. 9. Schematic arrangement of sites along the 10ℓ rows, which lie in the (010) plane for the lattices of (a) $3R$ (γ) + NH and (b) $3R + NR$. Dashed lines indicate the location of sites of the fcc and hcp structures. (c) Schematic arrangement of reflections in the electron diffraction pattern along the rows of 01ℓ type in the $(100)_{NR}$ plane of reciprocal rhombohedral N-layer lattice in a hexagonal system of axes.

lattice (Figs. 9a, 9b): with an increase in number of layers per unit cell, the sites arranged along the 10ℓ rows and the corresponding reflections in the electron diffraction pattern are located more often in both NH and NR phases. However, any NH structure yields the reflection 100, whereas this reflection is absent in the NR diffraction pattern.

In addition, the interpretation of electron diffraction patterns is facilitated by the following experimental fact (verified by calculation): if very strong maxima are located near fcc lattice reflections, the structure is mainly "cubic" (slightly deteriorated by hexagonal layers) and, vice versa, if strong reflections are situated near hcp lattice reflections, the structure consists mainly of hexagonal layers with a small number of cubic ones.

The schematic arrangement of reflections in the (100) plane of $18R$ phase is shown in Fig. 9c. Note that the R-phase reflections are located asymmetrically relative to both the c^* and b^* axes. Therefore, if twinning over (100), (010), (110), or (001) planes occurs in martensite plates, it should manifest itself in the formation of dual reflections in the electron diffraction pattern. Since the ε-martensite reflections are arranged symmetrically relative to these axes (Fig. 9a), twinning should not lead to their splitting.

Using these data, we will return to interpretation of the electron diffraction pattern in Fig. 7a. This pattern, in terms of our interpretation, is presented in Fig. 7c. One can see diffuse rods of three directions (denoted by different lines), which indicate the presence of randomly located stacking faults in the structure of dispersed martensitic-phase crystals. A system of parallel equally spaced rods oriented in the same direction is formed by dispersed crystals, also oriented in the corresponding direction.

The trace of the habit plane of martensitic-phase dispersed crystals is orthogonal to the corresponding diffuse rods; it follows from a comparison of Figs. 7b and 7c and is explained by the orthogonality of direct and reciprocal lattices (Fig. 8). It is fairly difficult to determine the R-phase type from the presented diffraction pattern because of the unfavorable orientation with respect to the electron beam. The lattice of the forming phase can be reliably determined when the arrangement direction of its close-packed planes coincides with the direction of primary electron beam and the site row 10ℓ lies in the screen plane. However, many indirect evidences also allow one to do this.

The diffuse rods whose direction is indicated by a line are most pronounced. The presence of small-angle misorientation in the system of these rods can be seen in the enlarged image of the reflection indicated by a black arrow and presented in the bottom inset. The top inset shows on an enlarged scale a group of reflections (indicated by a white arrow) located on the zero (passing through the 000 spot) rod, corresponding to the 00ℓ site row of the reciprocal lattice of multilayer phases in the hexagonal system of axes. A calculation showed that the weak reflection, split in the azimuthal direction, corresponds to d_{011} of the α phase; it is a manifestation of the distortion of the modulated structure matrix, arising due to the contraction displacements of {110} planes in the initial stage of formation of a denser structure. Along with the $\bar{2}00$ reflection, shaped as a diffuse arc, it forms a cell of the reciprocal lattice of α phase with the zone axis $[01\bar{1}]_\alpha$, indicated by a small-dotted line in the electron dif-

fraction pattern. Three reflections with a close interplanar spacing d are located near the 011_α reflection in the diffraction pattern; one of them is closer to the zero spot than the other two. These reflections correspond to three structural components: γ phase and two R phases with a small misorientation. The γ-phase reflection does not exhibit misorientation of dispersed plates, because the same $1\bar{1}\bar{1}_\gamma$ reflection belongs to both rods. Therefore, the reflection that is not split because of the small misorientation of dispersed plates characterizes the interplanar spacing d_{111} of the γ phase and corresponds to a larger d value. Therefore, the fcc γ phase is not the closest packed structure in this case. A similar experimental fact was also established for the γ phase entering the structure of large extended plates formed in stage III of the α → γ reverse transformation [11, 12].

Strong reflections of the multilayer phase are located near the $1\bar{1}\bar{1}_\gamma$ reflection (and on both strands) from both sides. Therefore, they belong to the R phase. According to Fig. 9b, these reflections are most likely formed by the 18R structure. Note that each reflection of the R phase is diffuse along the diffuse rod. This effect may be due to only twinning of the rhombohedral lattice, which leads to splitting of reflections on a diffuse rod because of their asymmetric arrangement relative to the zero rod (Fig. 9c). This experimental fact confirms the presence of regions with a rhombohedral lattice (along with the γ phase) in γ-martensite crystals.

A site row of the reciprocal lattice of 18R structure is shown on the right side of the electron diffraction pattern; this row is oriented parallel to the diffuse rod on the corresponding scale: horizontal lines show identical arrangement of the 200, 111, and 311 reflections of γ phase. Having compared the arrangement of multilayer-phase reflections in the diffraction pattern and in the site row, one can see a correspondence and the same value of gap between the reflections and their projection onto the site row. Therefore, one can conclude with high reliability that the multilayer martensite phase corresponds to the 18R structure. Thus, the analysis of the reported electron diffraction pattern shows that the orientation of distorted α matrix corresponds to the zone axis $[01\bar{1}]$ and that the basal planes $(111)_\gamma$ and (001)18R are formed in the $(011)_\alpha$ plane. The $(011)_\alpha$ and $(111)_\gamma$ planes are not strictly parallel: $(011)_\alpha \sim \|(111)_\gamma\|(001)_{18R}$. The orientations of the α and γ phases indicated in Fig. 7a are erroneous.

Note the reflection interpreted as the superstructural reflection $\bar{1}10_\gamma$ in the electron diffraction pattern (Fig. 7a). The existence of this reflection is considered important in [7, 8]: it indicates occurrence of diffusive redistribution of nickel atoms between the α matrix and γ-martensite crystals, which leads to their enrichment with nickel and formation of ordered $L1_0$ phase.

The location of this reflection strictly corresponds to the ε-phase structure. It is situated in the basal plane of reciprocal γ + ε lattice (Fig. 8d), at the intersection of diffuse 10ℓ rod with the basal plane (001). Its projection onto the site row (indicated by a prime), located somewhat higher the $10\bar{1}$ reflection of the 18R phase, corresponds to the 100_ε reflection, which was indexed due to the joint consideration of the reciprocal lattices presented in Figs. 8d and 8e. Thus, the structure of the martensitic dispersed crystals of the intermediate multilayer phase, formed at 430°C, contains layers of γ, ε, and 18R phases.

The current experimental result (most satisfactory to date) is presented in Fig. 10a: the electron beam is almost parallel to the basal plane $\{001\}_R$. The structure image was obtained for a sample of Fe–31%Ni alloy in the α + γ state, which was subjected to slow heating to 470°C. The corresponding electron diffraction pattern is presented in the inset. It is reproduced on an enlarged scale in Fig. 10b, where the periodicity of reflections on diffuse rods is more pronounced. There are six reflections between 220_γ and $11\bar{1}_\gamma$. Using the relationship $N = 3n$ [21], where N is the number of close-packed layers per rhombohedral-structure unit cell and n is the number of multilayer-phase reflections between two neighboring reflections of the fcc lattice, we find that $N = 3 \times 6 = 18$. Therefore, the dispersed-phase structure formed upon slow heating via the shear mechanism in the beginning of the temperature range of reverse α → γ transformation has a multilayer crystalline (3R + 18R) lattice. The scheme in Fig. 10c presents interpretation of its reflections and the corresponding orientation, which made it possible to determine the number of layers per R-phase unit cell. The $1\bar{1}25_{18R}$ and $1\bar{1}7_{18R}$ reflections have maximum intensity and are located near the 220_γ and $11\bar{1}_\gamma$ reflections, respectively, in the γ-phase reciprocal lattice. This circumstance makes it possible to index other reflections of the 18R phase, indicated by primes in the scheme.

The same electron diffraction pattern demonstrates diffuse rods oriented in two more directions. Each rod exhibits additional reflections, which belong to neither α nor γ phase but are manifestations of the multilayer martensite phase. However, the resolution was reduced because of the larger deviation of the basal planes {001} of R phase from the primary electron beam direction. One can see also three different orientations of extended plates of the intermediate martensite phase and the fourth orientation, presented by a cross section of rounded shape, in the corresponding structure image. Thus, an intermediate rod-like phase with four orientations is present in the structure of one α plate.

Note that the trace of the habit plane of extended rods (indicated by an arrow) is parallel to the twinning-plane trace in the rods oriented at a large angle

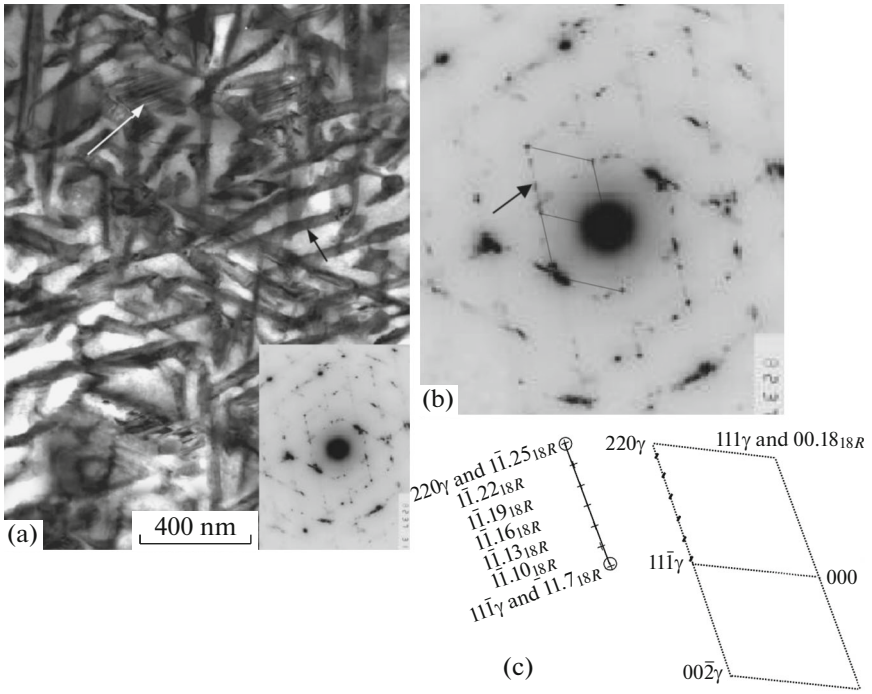

Fig. 10. (a)Image of particles of the intermediate phase formed in Fe–31%Ni alloy during slow heating with a rate of 0.2 K/min to 470°C (electron diffraction pattern in the inset) [8], (b) enlarged electron diffraction pattern, and (c) its interpretation scheme.

with respect to the drawing plane (indicated by a white arrow). Therefore, twinning occurs over the basal plane $(001)_R \| (111)_\gamma$.

Figure 11a [3] presents the alloy structure after heating to 480°C at a rate of 0.2 K/min. A noteworthy feature is the presence of clear striations oriented parallel to the habit of dispersed plates of γ martensite (a manifestation of its multilayer lattice, formed by the periodic arrangement of stacking faults), and accommodation twins periodically arranged in the plates. Twin interlayers were formed over planes coinciding with the martensite habit plane $(00\ell)_{18R} \| (111)_\gamma$, as well as in the previous structure (Fig. 10). The same type of twinning is presented in Fig. 11b (indicated by a dash-and-dot line). Note that twinning occurs also over another system. There are two lines in Fig. 11a; the first is parallel to the habit of γ-martensite crystal, and the second is parallel to the twinning plane of the second system (reproduced in the inset). The angle between them is exactly 120°. This fact suggests that twinning occurred over the (100) plane of the $3R$ + $18R$ phase, because the angle between the (100) and $(0\bar{1}0)$ planes is specifically 120° (Fig. 8f).

Therefore, accommodation twinning of the $3R$ + $18R$ phase is implemented both over the (00ℓ) basal planes and over (010), (100), or (110) planes. This experimental fact was presented for the NR phase for the first time. Twinning of this type should also lead to splitting of reflections in the electron diffraction pattern, but with rotation by 120° rather than 180°. Therefore, the reflections will look like tilted primes. This can be seen in Figs. 3c and 10b. In the electron diffraction pattern (Fig. 3c), along with circles containing reflections, direct segments indicate also regions demonstrating periodically arranged reflections in a straight-line series, which are a manifestation of an intermediate phase with a multilayer $18R$ lattice (whose basal plane is oriented parallel to the electron beam axis), which underwent twinning over the (11ℓ) plane.

Nikolin [21] proposed (based on the results of intrinsic experimental study and analysis of the corresponding data in the literature) a hypothesis, according to which multilayer martensite phases arise only in alloys having a limited homogeneity range of solid solution and undergoing (due to this feature) a homogeneous decomposition. If an alloy is a homogeneous solid solution, a direct martensitic transformation gives rise to a phase with an hcp lattice, and shifts necessary for transformation occur after each second close-packed layer $\{111\}_{fcc}$.

In the case under consideration the α matrix contains fine-grained (on the order of several lattice periods) particle of the Fe_3Ni phase, randomly distributed over the entire α-crystal volume; these particles form elastic stresses in the matrix. The latter retard shifts of atomic planes, which promote formation of an hcp lattice. As a result, close-packed planes shift without any strict order during the phase transition, and a martensite phase with several structures (ε and $18R$) arises.

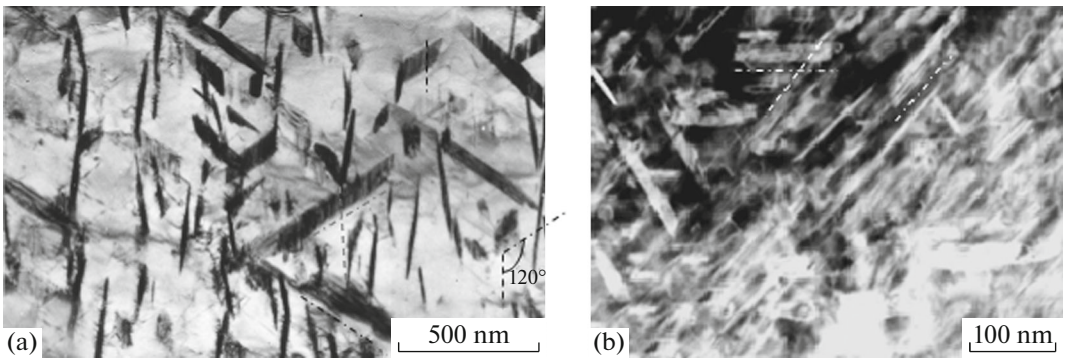

Fig. 11. Accommodation twinning of dispersed 18*R*-phase crystals formed in Fe–32%Ni alloy upon slow heating with a rate of 0.2 K/min to (a) 480°C, over planes parallel to the crystal habit (dash-and-dot line) and nonparallel to it [3] (angle 120° between the 18*R*-phase habit and the twinning plane), and (b) to 450°C over planes parallel and nonparallel to the crystal habit.

Thus, the hypothesis (stated in [21]) about the possibility of forming multilayer lattices in only inhomogeneous alloys, containing excess-phase particles or exhibiting stratification, was confirmed in this study.

The mechanism of forming multilayer lattices of martensite phases, proposed in [21], refers to the situation where the matrix is an fcc structure. In the case under consideration the intermediate phase of martensitic origin is formed in a bcc matrix. Hence, a question arises: why the fcc phase is present in the structure of dispersed crystals of the intermediate phase, which is equilibrium for the given system of metastable Fe–Ni alloys? We state the following hypothesis.

A transition from one phase to another is known to be accompanied by a step change in the internal energy, entropy, and volume, as well as by the absorption or release of a corresponding amount of heat. The behavior of the calorimetric curve starting with 380°C obeys this rule: it becomes jagged (Fig. 1). The jag amplitude increases and reaches a maximum in the range of the most active formation of dispersed new-phase crystals: 400–430°C. Figure 1b shows on an enlarged scale (extended along the temperature scale) this fragment of the calorimetric curve, which demonstrates a complicated stepwise (periodic) character of change in the α-crystal structure. This fragment contains eight sharp minima, corresponding to heat absorption (Fig. 1b). Let us discuss the behavior of the calorimetric curve between two minima by an example of the range of 400–404°C (Fig. 1c). It consists of five (enumerated) steps. The first minimum reflects the formation of a new phase, which requires the highest energy expenditure: this is an fcc phase (γ). The elevated coherent-stress energy relaxes via periodic shifts of (111) atomic planes in the γ phase, which leads to heat release: a sharp burst is observed in the calorimetric curve. Thus, conditions for developing a phase transformation inside dispersed plates (formation of ε-structure fragments) are created. This is the second stage in the calorimetric curve, which demonstrates necessity of heat supply from outside (alloy heating) and its subsequent absorption, but less intense than in the first stage. Then the third stage occurs: a small amount of heat is supplied again with its subsequent absorption and formation of an 18*R* structure. The large difference in the free energies of α and (γ + ε + *R*) phases at the transformation temperature facilitates development of twinning as an accommodation deformation mechanism, because twin nucleation may occur only at high stresses (on the order of 1/20 shear modulus) and preliminary accumulation of rather high elastic energy [30]. Therefore, relaxation twinning over the planes parallel to the crystal habit occurs in the newly formed complex structure of the intermediate phase; this is the fourth stage. The final, fifth stage is the relaxation twinning over one of the systems of planes making an angle of 120° with the habit plane.

Relaxation processes are a necessary component of the α → γ transformation. In their absence the increasing level of elastic coherent stress would lead to structure stabilization and impede nucleation of new γ-martensite plates in the α matrix.

With an increase in the heating temperature, after the relaxation processes in the primarily formed crystals of dispersed intermediate phase, the α-matrix stability decreases, and conditions for nucleation of second-turn γ-martensite plates and their growth (accompanied by relaxation phenomena) arise. Then the third turn of nucleation and growth of new intermediate-phase plates occurs, etc. Eight such "turns" were detected in the case considered here (Fig. 1b).

The number of these "turns" is not infinite. A rather high elastic coherent stress is accumulated in the α matrix. The alloy yield stress is twice as high as that in the initial state [3]. The α → γ transformation according to this mechanism stops.

The subsequent relaxation of elastic stress occurs via the formation of large extended new-phase plates, which are revealed metallographically; they are weakly etched against the background of initial α martensite and are often oriented parallel to each other or shaped

as frames, which is characteristic of athermal formation kinetics [11, 12, 31]. The absence of a sharp minimum in the temperature range of 440–450°C, which is due to the heat absorption during nucleation of large extended plates, is likely related to the sample heating rate, turned out to be high for detection. The dominant heat release, accompanying relaxation phenomena in the structure of large extended plates [31], overlaps the narrow range of their nucleation.

CONCLUSIONS

Thus, the comparison of the structure formed in samples of metastable Fe–Ni alloys (existing initially in the $\alpha + \gamma$ state) during slow heating at a rate of ~0.3 K/min with the calorimetric curve behavior revealed a complex multistep process of the formation of dispersed intermediate martensitic phase in the beginning of the temperature range of transformation of the initial α phase.

The transformation of an α crystal during slow heating in metastable Fe–Ni alloys begins with the formation of a modulated structure by contraction displacement of (110)-type planes along the [110] direction. This process is activationless; it occurs without energy expenditure and is implemented in Fe–(31–32) at % Ni alloys in the temperature range of 370–400°C. This experimental fact was disclosed for the first time.

The nucleation and growth of intermediate martensite phase particles begin in the regions of disclination rotation of α-martensite blocks, characterized by enhanced energy of elastic internal stress; these processes occur in the range of 380–400°C.

The particles of intermediate martensite phase in α-martensite blocks are formed against the background of a modulated structure. The particle habit coincides with the $(110)_\alpha$-type planes responsible for the modulated structure. There are six (110)-type planes in the bcc lattice. Therefore, particles of intermediate martensitic phase with only six different orientations can be formed. An analysis showed that the phase structure corresponds to $\gamma + \varepsilon + 18R$. Based on the analysis of the periodic step calorimetric curve, it was suggested that the nucleation of dispersed crystals begins with the nucleation of γ-martensite plates, which undergo relaxation coherent elastic stress by periodic shears, leading successively to the formation of ε and $18R$ regions in these plates. More complete relaxation of elastic stress in the structure of dispersed intermediate-phase crystals occurs via twinning both over the basal plane (parallel to the habit) and over the planes making an angle of 120° with it.

Thus, after the second stage of the $\alpha \rightarrow \gamma$ transformation, the fine intricate internal structure of dispersed γ-martensite particles consists of γ-, ε-, and $18R$-phase plates, undergoing joint relaxation twinning.

The experimental results of this study confirmed the hypothesis stated in [21], according to which the formation of multilayer lattices of martensite phases occurs only in initially inhomogeneous structures and is reduced to forbiddenness of some shears of close-packed $\{111\}_{fcc}$ planes. Dispersed precipitates of the Fe_3Ni phase, passing to the γ-martensite structure, generate elastic stresses, which hinder the shears of atomic planes that should lead to the formation of an hcp lattice. Shears are blocked in particular slip planes, as a result of which structures with different numbers of layers per unit cell arise.

It was established for the first time in this study that the formation of intermediate long-period martensite phase occurs from the very start of martensite crystal transformation upon heating. It is necessary to perform additional purposeful investigations to obtain clear microdiffraction patterns with orientation of $\{110\}_\alpha$-type planes parallel to the incident electron beam.

FUNDING

This study was performed within a government contract for the Institute of Metal Physics of the Ural Branch of the Russian Academy of Sciences, subject "Structure" (no. AAAA-A18-118020190116-6).

CONFLICT OF INTEREST

The author declares that she has no conflict of interest.

REFERENCES

1. V. D. Sadovskii, *Structural Inheritance in Steel* (Metallurgiya, Moscow, 1973) [in Russian].
2. K. A. Malyshev, V. V. Sagaradze, I. P. Sorokin, et al., *Transformation-Induced Hardening of Austenitic Alloys on Iron-Nickel Base* (Nauka, Moscow, 1982) [in Russian].
3. V. V. Sagaradze and A. I. Uvarov, *Hardening and Properties of Austenitic Steels* (RIO UrO RAN, Yekaterinburg, 2013) [in Russian].
4. V. G. Gorbach, E. A. Izmailov, and I. S. Panpanza, Fiz. Met. Metalloved. **34** (6), 1238 (1972).
5. V. V. Sagaradze, K. A. Malyshev, Yu. A. Vaseva, and L. V. Smirnov, Fiz. Met. Metalloved. **37** (5), 1051 (1974).
6. V. V. Sagaradze, K. A. Malyshev, V. M. Schastlivtsev, et al., Fiz. Met. Metalloved. **39** (6), 1239 (1975).
7. I. G. Kabanova, V. V. Sagaradze, N. V. Kataeva, and V. E. Danil'chenko, Fiz. Met. Metalloved. **112** (4), 404 (2011).
8. V. V. Sagaradze, N. V. Kataeva, I. G. Kabanova, et al., Fiz. Met. Metalloved. **115** (7), 704 (2014). https://doi.org/10.7868/S0015323014070080
9. N. D. Zemtsova, Tech. Phys. **59** (8), 1141 (2014).
10. H. Kessler and W. Pitsch, Arch. Eisenhüttenwesen **39** (3), 223 (1968).

11. N. D. Zemtsova, Crystallogr. Rep. **59** (3), 369 (2014).
12. N. D. Zemtsova, Zh. Tekh. Fiz. **84** (8), 46 (2014). https://doi.org/10.21883/0000000000
13. A. E. Vol, *Structure and Properties of Binary Metal Systems,* Vol. 2 (Fizmatlit, Moscow, 1962) [in Russian].
14. A. Chamberod, J. Laugier, and J. M. Penisson, J. Magn. Magn. Mater. **10** (2–3), 39 (1979).
15. N. D. Zemtsova, Usp. Fiz. Nauk, **188**, 1103 (2018). https://doi.org/10.3367/UFNr.2018.02.038298
16. N. D. Zemtsova, Zh. Tekh. Fiz. **91** (7), 1139 (2021). https://doi.org/10.21883/JTF.2021.07.50955.344-20
17. N. D. Zemtsova, Tech. Phys. **62** (5), 731 (2017).
18. N. D. Zemtsova, Tech. Phys. **62** (6), 871 (2017).
19. V. D. Sadovskii, In *Structural Mechanism of Phase Transformations of Metals and Alloys* (Nauka, Moscow, 1976) [in Russian], p. 5.
20. D. A. Mirzaev, K. Yu. Okishev, and I. L. Yakovleva, Vestn. YuUrGU, Ser. Metall. **16** (2), 55 (2016). https://doi.org/10.14529/met160208
21. B. I. Nikolin, *Multilayer Structures and Polytypism in Metal Alloys* (Naukova Dumka, Kiev, 1984) [in Russian].
22. V. V. Sagaradze, V. A. Shabashov, V. E. Danilchenko, and P. L'Heritier, Mater. Sci. Eng. A **337**, 146 (2002).
23. N. D. Zemtsova, I. G. Kabanova, and E. I. Anufrieva, Fiz. Met. Metalloved. **105** (1), 23 (2008).
24. V. P. Skripov and A. V. Skripov, Usp. Fiz. Nauk **128** (2), 193 (1979).
25. K. V. Chuistov, Metallofizika, No. 32, 38 (1970).
26. F. A. Kassan-Ogly, V. E. Naish, and I. V. Sagaradze, Fiz. Met. Metalloved. **65** (3), 481 (1988).
27. M. P. Kashchenko and V. G. Chashchina, Fiz. Met. Metalloved. **116** (10), 1011 (2015). https://doi.org/10.7868/S001532301510006X
28. D. A. Mirzaev and S. V. Rushits, Fiz. Met. Metalloved. **37** (5), 912 (1974).
29. E. A. Pilyankevich, A. I. Ustinov, and K. V. Chuistov, Kristallografiya **27** (5), 881 (1982).
30. A. G. Khachaturyan, *Theory of Phase Transformations and Structure of Solid Solutions* (Nauka, Moscow, 1980) [in Russian].
31. N. D. Zemtsova, Crystallogr. Rep. **62** (1), 97 (2017).

Translated by Yu. Sin'kov